Variable DC-link Control Strategy for Maximum Efficiency of Traction Motor Drives

Variable DC-link Control Strategy for Maximum Efficiency of Traction Motor Drives

Paolo Pescetto
Department of Energy Galileo Ferraris Politecnico di Torino, Torino, Italy
paolo.pescetto@polito.it

Andres Sierra-Gonzalez
TECNALIA, Basque Research and Technology Alliance (BRTA)
Bilbao, Spain
andres.sierra@tecnalia.com

Elena Trancho
TECNALIA, Basque Research and Technology Alliance (BRTA)
Bilbao, Spain
elena.trancho@tecnalia.com

Gianmario Pellegrino
Department of Energy Galileo Ferraris Politecnico di Torino, Torino, Italy
gianmario.pellegrino@polito.it

***Abstract*—This work proposes an optimized control strategy for online adapting the DC-link voltage in a traction motor drive. In the considered vehicle architecture, a DC/DC converter boosts the battery voltage (rated 400 V) to a controlled DC-link, which feeds the traction inverter. The amplitude of the DC-link is online varied depending on the drive speed and torque conditions to minimize the power losses in the DC/DC converter and in the traction inverter. The switching losses in both the converters are reduced by minimizing the DC-link voltage without affecting the motor control performance. The proposed DC-link adaptation technique is almost independent of the motor parameters and adopted torque/speed control strategy, therefore it can be adopted in a wide number of applications. Moreover, it requires minimal calibration effort.**

***Index Terms*—Electric vehicles, Variable DC-link, Motor drives, DC/DC converter, Efficiency improvement, Loss minimization**

I. Introduction

The recent trend in road transportation presents a constantly growing share of electric and hybrid vehicles [1], leading to relevant business opportunities together with technological challenges. The drive efficiency is a major Key Performance Indicator (KPI) of the Battery Electric Vehicles (BEVs), with significant impact in terms of cooling requirements, rated power, overload capability [2] and e-axle compactness.

Among the recent technological trends, the growing power ratings and reliability requirements push for the adoption of multi-three phase drives, already widely present in high power applications such as wind turbines, ship propulsion and aerospace [3], [4]. In particular, in the automotive sector the 6-phase solution offers a good trade-off between improved motor performance and increased complexity of the drive, and has been recently explored by several research projects [5]–[7].

One of the most critical element of any BEV is the traction battery. Safety and isolation requirements push for a low voltage battery, whereas the increasing speed rating of the traction drives requires a high voltage to improve the machine speed range. Additionally, a high DC-link voltage normally permits a better efficiency of the drive thanks to the lower current rating.

To solve the trade-off, the EV under test [6] presents a DC/DC converter between the battery and the traction inverter, permitting to regulate the inverter DC-link voltage in the 800 V range despite a battery voltage rated 400 V. This helps to improve the motor control dynamic at high speed without the need of a very high voltage battery, which often presents technological issues. Moreover, the DC/DC converter permits embedded compatibility with DC fast charging stations [6]. On the other side, the DC/DC converter necessarily introduces additional conduction and switching losses during driving, affecting the EV's efficiency.

A feasible solution to reduce the additional losses is to online adapt the DC-link voltage during driving on varying the operating point of the machine [8]. The adaptation of the DC-link voltage is also beneficial for reducing the iron losses in the machine [9]. Anyway, most of the DC/DC control techniques proposed in literature [8], [10]–[15] require a fast dynamic variation of the DC-link, to adapt it on varying the rotor position. This can be achieved only if the DC/DC and

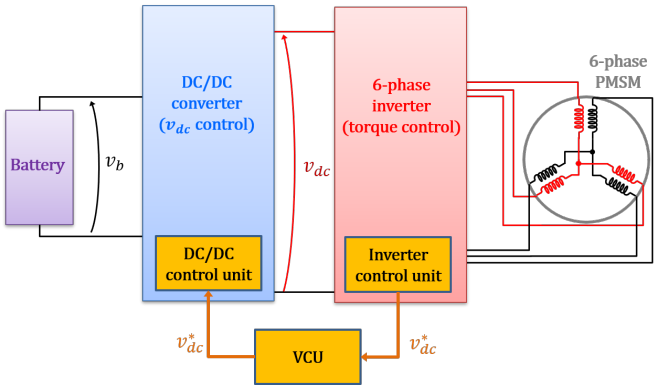

Fig. 1. Considered EV powertrain [5].

This project has received funding from the European Union's H2020 research and innovation programme under Grant Agreement no. 824335.

TABLE I
E-AXLE SPECIFICATION.

DC/DC converter		
Battery voltage	320÷420	V
Max v_{dc}	750	V
Max continuous power	180	kW
e-Drive		
Number of phases	3÷6	(configurable)
Switching frequency	12	kHz
Continuous torque	80	Nm
Peak torque	170	Nm
Continuous power	70	kW
Peak power	135	kW
Max speed	22000	rpm
Max current (6-phase)	235	Arms

the inverter are integrated into the same converter, so the motor control and the DC/DC control are executed in the same control board with negligible delay. Moreover, techniques like [8], [10]–[14] are only applicable if the motor control is custom designed together with the DC/DC control, so the torque control strategy is constrained and cannot be chosen arbitrarily. Additionally, methods such as [10], [13], [14] exploit non-standard DC/DC converters, which may not be accepted for large scale automotive production.

This work proposes an optimized DC-link control strategy able to minimize the losses in the DC/DC converter and in the traction inverter without limiting the motor control dynamic performance. The DC-link voltage is properly online adapted during driving to minimize the losses in the two converters. A key advantage of the proposed algorithm is that the motor control and the DC/DC converter are treated as independent black boxes, so it is applicable whatever the adopted torque control strategy. This permits to develop, debug and calibrate the two algorithms separately, with large freedom for the choice and calibration of the torque control. Moreover, the developed DC/DC control does not depend on the type, ratings or number of phases of the electrical machine, so it is applicable also for multi-three phase drives. Finally, the proposed method can be implemented independently by DC/DC converter structure, which can be integrated with the inverter or not.

In turn, the proposed adaptive DC-link control has been designed for a specific EV architecture equipped with a 6-phase motor drive, but it can be considered an add-on to the torque control algorithm in a wide range of electric drive applications, not limited to the automotive sector.

II. VEHICLE ARCHITECTURE

The considered powertrain, designed for an A-segment EV [6], is shown in Figure 1, while Table I reports its main ratings. The DC/DC converter boosts the battery voltage v_b from a rated 400 V to a regulated v_{dc} up to 750 V, feeding the 6-phase inverter and ultimately the dual-three phase Permanent Magnet Synchronous Motor (PMSM). The PMSMs are the most commonly adopted motor type in automotive thanks to their high efficiency and torque density, despite their non-linear magnetic saturation characteristic [16].

For testing purposes, the two 3-phase sets of the PMSM can be connected in parallel, forming a standard 3-phase machine. This possibility was exploited in this work: the optimal DC-link control was first developed and tested on the equivalent 3-phase motor and then extended to the 6-phase case.

The adopted commercial DC/DC [17] is an automotive grade bidirectional boost converter, therefore the v_{dc} is regulated in the range:

$$1.1 \cdot v_b < v_{dc} < 750V \tag{1}$$

According to the specifications detailed in Table I, the battery voltage depends on its State Of Charge (SOC), varying between 320 V and 420 V with a rated value v_b=370 V. For simplicity, a minimum v_{dc} of 400 V will be considered in this work, without loss of generality.

For a given torque reference T^* required by the driver and the measured vehicle speed, the 6-phase inverter controls the torque at the shaft, while the DC/DC converter regulates the DC link voltage for loss minimization (see Figure 1). The two converters are physically separated, without any direct communication between them. The proposed variable v_{dc} algorithm, executed in the Inverter Control Unit (ICU), computes the reference v_{dc}^*, which is communicated via CAN protocol to the Vehicle Control Unit (VCU) and ultimately to the DC/DC control unit. This communication introduces a relevant delay of 20÷22 ms between the v_{dc}^* determination and its execution. Moreover, the DC/DC converter presents an additional internal response time of 3 ms. Such very high communication and execution delay is dominating the dynamic performance of the v_{dc} control. Therefore, the implementation of methods like [8], [10]–[13] is not possible, as they require a sufficiently high v_{dc} control bandwidth to adapt the DC-link on varying the rotor position.

A. Efficiency Maps of the Converters

The first step for developing the adaptive DC-link control strategy is to analyze the efficiency characteristics of the inverter and the DC/DC converter on varying v_{dc}. Dealing with the inverter, the amplitude of v_{dc} has negligible effect on the conduction losses, but a low bus voltage can effectively reduce the switching losses. Therefore, the inverter efficiency increases at lower v_{dc}.

Similarly, for a given output power, a lower v_{dc} reduces the switching losses in the DC/DC converter, but the higher output current increases the conduction losses. Therefore, determining the optimal v_{dc} minimizing the DC/DC losses may be not trivial. Anyway, the switching loss reduction is commonly predominant, and after deep analysis, also the efficiency of the adopted commercial DC/DC converter [17], results higher by reducing v_{dc}.

The power loss characteristics of the two converters on varying the DC-link voltage are reported in Figure 2 for

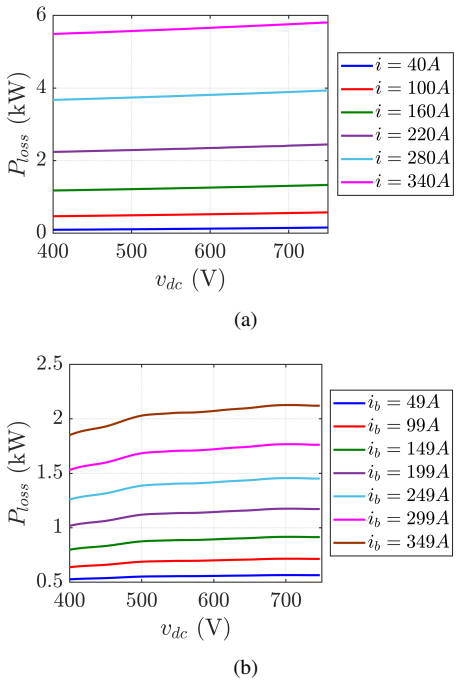

Fig. 2. (a) Power losses in the 6-phase inverter for different phase current amplitude and (b) in the DC/DC converter on varying the battery current, considering the rated battery voltage v_b=370V.

different current levels. As can be noted, for a given motor power, the losses in both converters increase with v_{dc}.

III. Motor Torque Control

This work focuses on the novel DC-link adaptation strategy, which is almost independent of the motor control algorithm. The only requirement is that the motor control must be capable of operating under a variable DC-link. For this reason, the adopted torque control strategies are only marginally described here, but further details can be found in [18]–[20].

To prove its substantial independence from the motor control, the proposed DC-link adaptation was tested when combined with two different torque control techniques, namely Current Vector Control-Field Oriented Control (CVC-FOC) [18], [20] and Direct Flux Vector Control (DFVC) [19]. Moreover, each of them have been tested both in 3-phase and 6-phase configuration.

In the CVC-FOC [18], commonly adopted in traction applications, the torque reference T^* is translated into an optimal current vector $\boldsymbol{i}^*_{\boldsymbol{dq}}$. The current is imposed to lay on the MTPA locus at medium and low speed and moving to field weakening when the maximum voltage reference is reached. In principle, the determination of the reference current vector depends on the reference T^*, set by the user, the measured speed n and the measured v_{dc}, thus requiring Look-Up Tables in three dimensions (3D LUTs). In this implementation, following [18], the complexity of the LUTs is reduced to two dimensions (2D LUTs) based on T^* and a manipulation of the measured speed, to consider the v_{dc} variability. This permits a reliable torque control in flux weakening even under relevant DC-link variations.

The second tested technique is the DFVC [19], where the controlled variables are the flux amplitude λ and its quadrature current i_{qs}, both closed loop imposed by dedicated PI controllers operating in stator flux coordinates (d_s, q_s). A hybrid flux observer (HFO) is implemented, merging the flux estimation based on the current model and the integration of the back-electromotive force. The direction of the observed flux vector in stator coordinates $\hat{\boldsymbol{\lambda}}_{\boldsymbol{\alpha\beta}}$ defines the d_s axis, shifted by the angle θ_s respect to the α direction. As usual, the q_s axis is 90° ahead of the d_s direction. The reference flux amplitude λ^* is set based on MTPA locus, and flux weakening is implemented by directly limiting λ^* based on the measured speed and DC-link voltage:

$$\lambda_{max} = \frac{\frac{v_{dc}}{\sqrt{3}} - R_s i_{qs} \cdot sign(\omega)}{|\omega|} \tag{2}$$

Figure 3 depicts the two adopted torque control strategies for a 3-phase machine. Both of them can be extended to the 6-phase case with dedicated algorithms [20].

As a final remark, both CVC-FOC and DFVC force the operating point on the MTPA below the base speed ω_b, in order to minimize the Joule losses, while field weakening is necessary at higher speed despite the lower efficiency of the machine. It should be noted that ω_b increases with the applied v_{dc}. Therefore, the motor Joule losses are reduced if the variable DC-link control adapts the v_{dc} (and so ω_b) permitting to operate on the MTPA.

IV. Variable DC-link Control Strategy

At first, the DC/DC control was developed for the equivalent 3-phase motor drive, considering the two 3-phase sets of the reference machine connected in parallel. In a second stage, the DC/DC control has been extended to the 6-phase case.

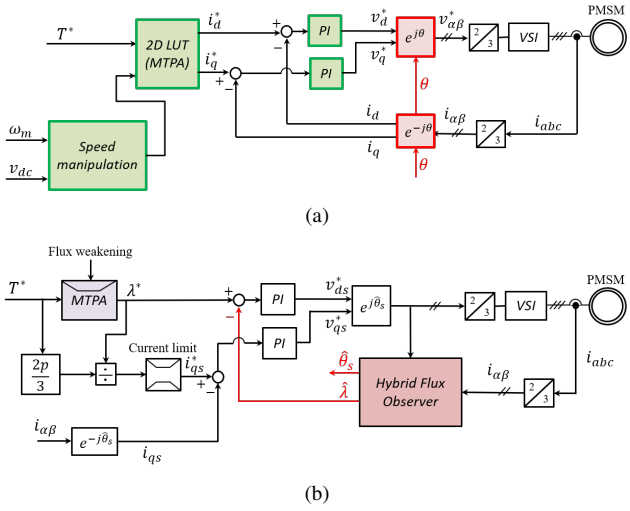

Fig. 3. Tested torque control algorithms. (a) CVC-FOC; (b) DFVC.

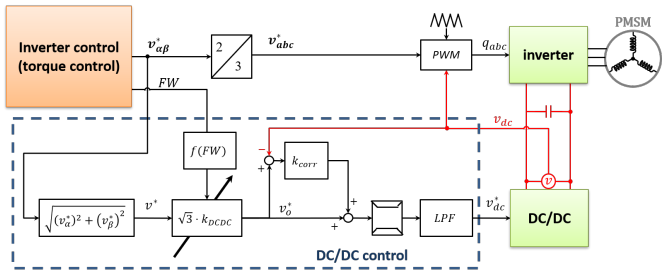

Fig. 4. Block scheme of the proposed DC-link control strategy for a generic 3-phase drive.

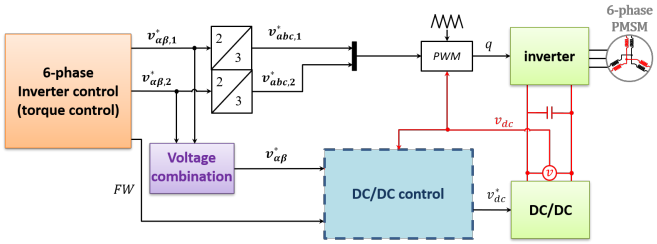

Fig. 5. Block scheme of the proposed DC-link control strategy extended to a 6-phase drive.

A. DC-link Control for a 3-phase Drive

The block scheme of the variable DC-link control is depicted in Fig. 4. The basic concept is to minimize the v_{dc} without affecting the motor control performance, i.e. avoiding unnecessary field weakening operation and without limiting the torque control bandwidth. According to the analysis in Section II-A this leads to the minimization of the power losses in the inverter and in the DC/DC converter without increasing the Joule losses in the machine, thus effectively improving the efficiency of the drive.

Whatever the adopted algorithm, the motor control outputs the reference voltage vector in stationary reference frame $\boldsymbol{v}^*_{\boldsymbol{\alpha\beta}}$, which is input to the DC/DC control block and used to define the reference v^*_{dc}.

For standard 3-phase PWM or Space Vector modulation techniques, the maximum amplitude of the voltage vector (peak of phase voltage) that can be synthesized is

$$|\boldsymbol{v}^*_{\boldsymbol{\alpha\beta}}|_{max} = v_{dc}/\sqrt{3} \tag{3}$$

Therefore, the amplitude of the $\boldsymbol{v}^*_{\boldsymbol{\alpha\beta}}$ vector is extracted and adopted to compute the signal v^*_o:

$$v^*_o = \sqrt{3} \cdot k_{DCDC} |\boldsymbol{v}^*_{\boldsymbol{\alpha\beta}}| \tag{4}$$

where $k_{DCDC} > 1$ is a scalar gain. The value of k_{DCDC} is online adapted based on the FW signal, which is a flag indicating if the torque control is working along the MTPA ($FW = 0$) or in field weakening speed range ($FW = 1$). In particular, k_{DCDC} is bounded between a minimum k^{min}_{DCDC} and a maximum k^{max}_{DCDC} value, and it is ramped up for $FW = 1$ and it is ramped down for $FW = 0$. In other words, $k_{DCDC} = k^{min}_{DCDC}$ when the drive is operating on the MTPA, and linearly increased up to $k_{DCDC} = k^{max}_{DCDC}$ under flux weakening operation.

Then, the difference between v^*_o and the measured v_{dc} is multiplied by the scalar gain k_{corr} and added to v^*_o. The obtained signal, saturated based on the DC/DC converter operating limits, is Low-Pass Filtered (LPF) to obtain the reference v^*_{dc}.

$$v^*_{dc} = LPF(v^*_o + k_{corr}\,(v^*_o - v_{dc})) \tag{5}$$

This operation permits increasing the DC/DC control dynamic during transient, i.e. when $v_{dc} \neq v^*_{dc}$, without significantly affecting the steady state performance.

Finally, v^*_{dc} is communicated to the DC/DC converter and executed, as said, with a significant delay of ≈25 ms, which must be considered at calibration stage.

B. Extension to 6-phase Drive

The variable DC-link control was successfully extended to the dual-three phase case, slightly complicating its algorithm, but without affecting its high performance.

The control block scheme is reported in Figure 5. Essentially, the same adaptive DC-link control strategy and calibration can be adopted as in the 3-phase case, but the input voltage vector $\boldsymbol{v}^*_{\boldsymbol{\alpha\beta}}$ is the aggregate of the reference voltages of the two 3-phase sets $\boldsymbol{v}^*_{\boldsymbol{\alpha\beta,1}}$ and $\boldsymbol{v}^*_{\boldsymbol{\alpha\beta,2}}$. It should be noted that the control calibration, bandwidth and performance are not modified respect to the 3-phase case.

The combination law of the two voltage vectors depends on the connection between the two 3-phase inverter units [18]. For parallel connected inverters, which is the most common solution, the input of the DC/DC control will simply be the voltage vector having larger amplitude:

$$|\boldsymbol{v}^*_{\boldsymbol{\alpha\beta}}| = max\left(|\boldsymbol{v}^*_{\boldsymbol{\alpha\beta,1}}|, |\boldsymbol{v}^*_{\boldsymbol{\alpha\beta,2}}|\right) \tag{6}$$

This condition permits to instantaneously guarantee sufficient v_{dc} to control both the 3-phase sets without affecting the torque control performance.

If the two 3-phase inverters are connected in cascade configuration [18] the DC/DC will need to control the total DC-link voltage, but the torque control must include a voltage balancing algorithm, to ensure the DC-link voltage is equally split between the two inverters [20]. In this case, a good combination law of the two reference voltage vectors is:

$$|\boldsymbol{v}^*_{\boldsymbol{\alpha\beta}}| = |\boldsymbol{v}^*_{\boldsymbol{\alpha\beta,1}}| + |\boldsymbol{v}^*_{\boldsymbol{\alpha\beta,2}}| \tag{7}$$

Overall, for a wide number of multiphase converters topologies a proper law for combining the reference voltage vectors of each 3-phase set can be easily found, confirming the wide applicability of the proposed variable DC-link control strategy.

C. Control Calibration

This section details the calibration roles of the proposed DC-link adaptation strategy, valid both for the 3-phase and for the 6-phase cases. The main parameters that need to be tuned are limited to the scalar gain k_{DCDC} and the cut-off frequency of the LPF, demonstrating the simplicity of implementation of this adaptive DC-link control.

The gain k_{DCDC} determines the voltage margin between v_{dc} and the inverter phase voltage. It should be noted that, at steady state, the DC-link voltage is given by:

$$v_{dc} = \sqrt{3}|\boldsymbol{v}^*_{\boldsymbol{\alpha\beta}}| \cdot k_{DCDC} \tag{8}$$

As an example, setting k_{DCDC}=1.1 guarantees 10% voltage margin. Its calibration is a trade off between control performance and optimal voltage utilization. At higher k_{DCDC}, a larger DC-link voltage margin is imposed, thus permitting to maintain stable torque control under faster acceleration of the motor. On the other side, a larger v_{dc} means the switching losses in the converters are not minimized. This trade off is essentially solved by using a variable k_{DCDC} based on the FW signal, where k^{min}_{DCDC} is calibrated for optimum voltage utilization and k^{max}_{DCDC} boosts the control dynamic during transients. In this implementation, the selected gains are k^{min}_{DCDC}=1.1 and k^{max}_{DCDC}=1.2.

The second parameter requiring calibration is the LPF cut-off frequency. Such LPF is necessary to avoid unstable or underdamped response, although it limits the bandwidth of the v^*_{dc} control. In practice, the feasible DC-link control bandwidth is limited by the communication delay and by the possible interaction with the motor control. For a reliable system, the LPF should be calibrated sufficiently slower than the torque control bandwidth. In this implementation, the LPF cut-off frequency was set at 30 Hz, to be compliant with a large number of torque control strategies. A higher control bandwidth is feasible, at the cost of possible oscillations in the v_{dc} response. This is acceptable only if the torque control is sufficiently robust under fast DC-link variations. More details are given in Section V.

V. Simulation Results

The proposed adaptive DC-link control was thoroughly validated in Matlab-Simulink environment using accurate modeling of the electrical machine and power electronic converters. This section reports the results of the DC-link control combined with different torque control strategies. For each test, the motor speed is externally imposed.

In each reported result, the slew rates of speed variation were set at +15000 rpm/s (correspondent to 135 (km/h)/s on the EV) in acceleration and -30000 rpm/s (i.e. -270 (km/h)/s) for breaking, while the torque reference variation is ramped with a slew rate of 1500 Nm/s. All these values are considerably higher than the feasible accelerations on the vehicle, to demonstrate the high control performance and robustness of the proposed technique.

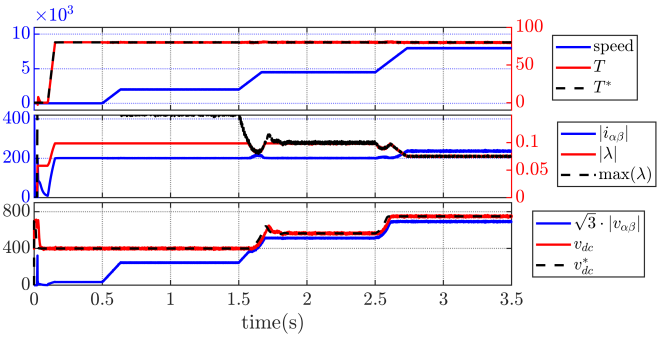

Fig. 6. Simulation of DC/DC control combined with CVC-FOC torque control for 3-phase configuration: steady state operation at rated torque and different speed (2000, 4500 and 8000 rpm).

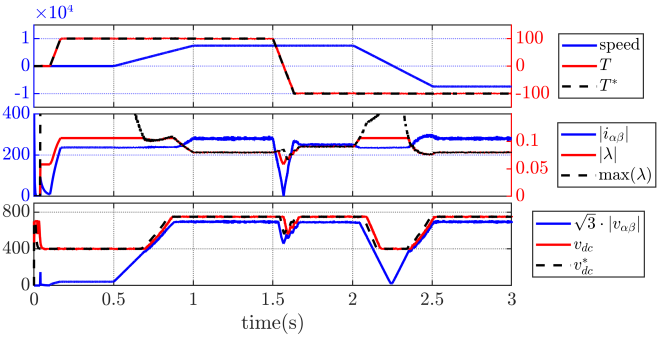

Fig. 7. Simulation of DC/DC control combined with DFVC torque control for 3-phase configuration: complex load cycle.

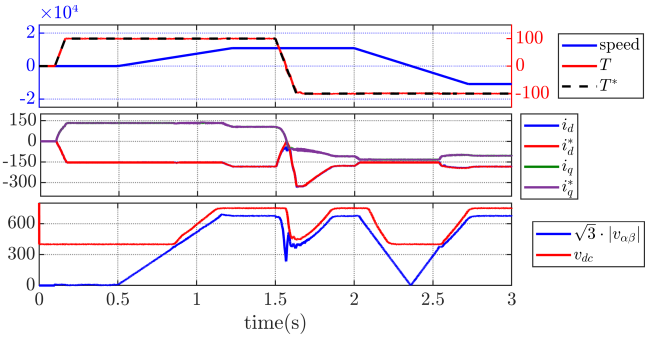

Fig. 8. Simulation of DC/DC control combined with CVC-FOC torque control for 6-phase configuration: complex load cycle.

A first test is depicted in Figure 6, where the motor is controlled in DFVC under 3-phase configuration [19]. The rated torque reference is demanded T^*=80 Nm, while three speed steps are imposed, moving the motor speed n from zero to 2000 rpm, then to 4500 rpm and finally to 8000 rpm. The upper subplot depicts the torque and speed transient. The middle subplot shows the flux and current amplitude, together with the maximum flux limit λ_{max} (black line). The DFVC operates on the MTPA when the reference flux is below the flux limit, whereas it imposes field weakening when $\lambda = \lambda_{max}$. The third subplot depicts the controlled DC-link voltage and the amplitude of the vector $\boldsymbol{v}^*_{\boldsymbol{\alpha\beta}}$ multiplied by

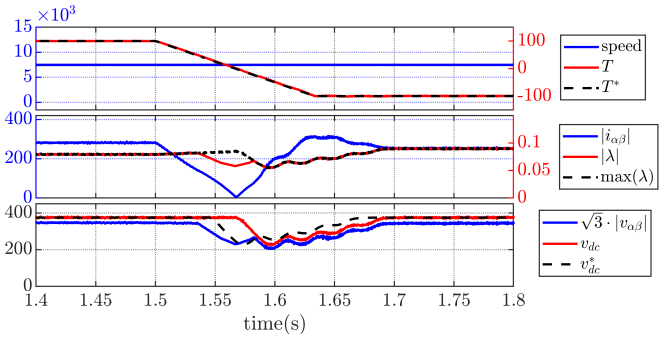

Fig. 9. Torque reversal at 7500 rpm, 100 Nm with a LPF cut-pff frequency of 30 Hz.

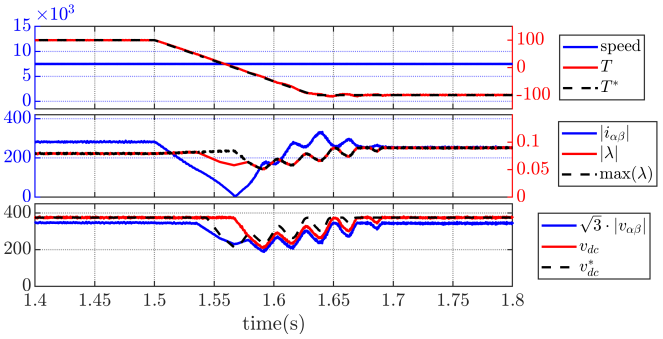

Fig. 10. Torque reversal at 7500 rpm, 100 Nm with a LPF cut-pff frequency of 150 Hz.

$\sqrt{3}$, i.e. the minimum DC-link voltage required to synthesize the reference $\boldsymbol{v^*_{\alpha\beta}}$. It should be noted that the measured v_{dc} (red line) follows the reference signal v^*_{dc} (black line) with a remarkable delay considering the communication and actuation delay.

As can be noticed in Figure 6, the drive presents three regions of steady state operation. At standstill and for n=2000 rpm, i.e. for t <1.5 s, the minimum DC-link voltage is sufficient for controlling the machine on the MTPA, therefore the command v^*_{dc} is saturated at its minimum value (400 V). At medium speed (4500 rpm, 1.5 s< t <2.5 s) the minimum v_{dc} is not enough to operate on the MTPA locus, and the motor control would tend to go into flux weakening region. This is avoided by increasing the DC-link to 580 V, slightly higher than the minimum required for maintaining the motor working point on the MTPA. The correct MTPA operation is confirmed by the same flux and current amplitude as the values obtained at 2000 rpm. For a speed of 8000 rpm or higher (t >2.5 s), the v^*_{dc} is saturated to its maximum limit (750 V), so the DC/DC is not able to further increase the DC-link voltage. At this point, flux weakening is physically unavoidable as the MTPA locus cannot be tracked. This results in a lower $|\lambda|$ and a higher current amplitude. Anyway, since the drive is operating at the maximum available v_{dc} the operating point is as close as possible to the MTPA locus.

Figure 7 depicts another example of simulation results for the machine in 3-phase configuration and controlled with DFVC, but under a complex operating cycle. The meaning of the reported signals is the same as described in Figure 6. The simulation starts at zero torque and speed. Then, a step of 100 Nm (25% overload) is demanded by the motor control. Since the motor is at standstill, at this point the variable DC-link control converges at the minimum v_{dc}, which is sufficient for operating on MTPA. Starting from t=0.5 s the motor is sharply accelerated to 7500 rpm, i.e. roughly 20% over the base speed. During the acceleration, as soon as the voltage reference gets close to saturation the variable DC-link control correctly reacts by increasing the v_{dc}, which is then saturated to the maximum value (750 V) unavoidably requiring field weakening on the motor. At t=1.5 s, the torque is reversed to -100 Nm. Despite the high speed, the torque transiently goes to zero before becoming negative. It can be noted that when the absolute value of T^* is low the required voltage is also reduced, the maximum v_{dc} is unnecessary and the variable DC-link control tends to decrease the v^*_{dc}. This results in a small drop in v_{dc}, promptly recovered as the negative torque increases. Finally, the speed is reversed to -7500 rpm at t=2 s. The v_{dc} is correctly reduced when the speed decreases, thus reducing the required voltage, and again increased when the speed increases in negative direction. In turn, the motor control is stable even under severe transients and/or flux weakening conditions, while the adaptive DC-link control properly imposes the minimum v_{dc}, avoiding flux weakening if possible.

A simulation of the variable DC-link control coupled with CVC-FOC motor control is depicted in Figure 8 for the 6-phase configuration [20]. The simulation was run under the same load cycle as in Figure 7, with sharp torque step and acceleration followed by torque and speed reversals. Also in this case, the control is working properly, with the reference torque accurately tracked and the v_{dc} correctly imposed at its minimum. The main difference respect to the DFVC case is a larger voltage sag under torque reversal. This can be explained considering the inherently higher capability of the DFVC of accurate and fast torque regulation under flux weakening respect to the CVC-FOC. In both cases, the motor control dynamic is not affected by the variable DC-link control, so the torque can be regulated at the best capabilities of the motor control algorithm.

Finally, the effect of LPF calibration is depicted in Figures 9 and 10, where the motor is still controlled in DFVC in 3-phase configuration. Both cases report a sharp torque reversal from +100 Nm to -100 Nm under constant speed (7500 rpm). The test in Figure 9 was performed with the same LPF calibration as Figures 6 and 7, i.e. a cut-off frequency of 30 Hz, while for the test reported in Figure 10 the filter was set at 150 Hz. As can be noted, this latter test presents a significant oscillation of the DC-link under severe torque variation. In this test, this oscillation is not affecting the torque control accuracy thanks to the inherent capability of the DFVC to follow the torque set-point, but it may be critical in other types of control, such as CVC.

A complete experimental validation of the proposed technique is currently ongoing. The experimental results will be soon included in future publications. The adopted setup is reported in Fig. 11, including the motor under test and the 6-phase inverter.

VI. Conclusions

This work proposes a simple and effective strategy for controlling the variable DC-link of an EV equipped with a DC/DC converter. The core of the algorithm is to online minimize the DC-link voltage on varying the drive operating point without affecting the motor control performance, thus permitting MTPA operation up to the maximum possible speed and without limiting the motor control bandwidth. The algorithm is independent from the adopted motor control strategy and can operate even if the inverter and the DC/DC converter are physically separated, despite the significant communication delay between the two. Therefore, the proposed variable DC-link control and the motor control can be developed and tested separately, permitting high flexibility and debugging options. Moreover, it is easily adapted to multi-three phase applications. Despite originally designed for EVs, the present technique can be applied to a wide number of applications presenting a controllable DC-link.

Acknowledgment

The authors are grateful to the European Commission for the support to the present work, performed within the EU H2020 project FITGEN (Grant Agreement 824335).

The research has been conducted with the support of Power Electronics Innovation Center (PEIC) of Politecnico di Torino.

References

[1] IEA, “Global EV Outlook 2020,” 2020. [Online]. Available: https://www.iea.org/reports/global-ev-outlook-2020. [Accessed June 23rd 2021].

[2] R. Leuzzi, P. Cagnetta, S. Ferrari, P. Pescetto, G. Pellegrino and F. Cupertino, ”Transient Overload Characteristics of PM-Assisted Synchronous Reluctance Machines, Including Sensorless Control Feasibility,” in *IEEE Transactions on Industry Applications*, vol. 55, no. 3, pp. 2637-2648, May-June 2019.

[3] E. Levi, ”Multiphase Electric Machines for Variable-Speed Applications,” in *IEEE Transactions on Industrial Electronics*, vol. 55, no. 5, pp. 1893-1909, May 2008.

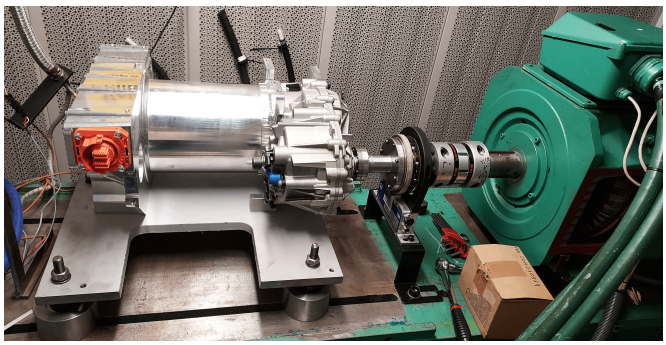

Fig. 11. Test bench for experimental validation of the proposed method, including the traction inverter and motor, the mechanical gearbox, the torque meter and the load machine.

[4] A. Boglietti, I. R. Bojoi, S. Rubino and M. Cossale, ”Overload Capability of Multiphase Machines Under Normal and Open-Phase Fault Conditions: A Thermal Analysis Approach,” in *IEEE Transactions on Industry Applications*, vol. 56, no. 3, pp. 2560-2569, May-June 2020.

[5] H2020 EU FITGEN project. Available: https://fitgen-project.eu/ [Accessed June 23rd 2021].

[6] M. Martino, P. Pescetto and G. Pellegrino, ”Advanced Functionally Integrated E-Axle for A-Segment Electric Vehicles,” *2020 AEIT International Conference of Electrical and Electronic Technologies for Automotive (AEIT AUTOMOTIVE)*, Turin, Italy, 2020, pp. 1-6.

[7] A. Salem and M. Narimani, ”A Review on Multiphase Drives for Automotive Traction Applications,” in *IEEE Transactions on Transportation Electrification*, vol. 5, no. 4, pp. 1329-1348, Dec. 2019.

[8] T. Schoenen, M. S. Kunter, M. D. Hennen and R. W. De Doncker, ”Advantages of a variable DC-link voltage by using a DC-DC converter in hybrid-electric vehicles,” *2010 IEEE Vehicle Power and Propulsion Conference*.

[9] K. Yamazaki and A. Abe, ”Loss Investigation of Interior Permanent-Magnet Motors Considering Carrier Harmonics and Magnet Eddy Currents,” in *IEEE Transactions on Industry Applications*, vol. 45, no. 2, pp. 659-665, March-april 2009.

[10] J. Lu, A. Mallik, S. Zou and A. Khaligh, ”Variable DC-Link Control Loop Design for an Integrated Two-Stage AC/DC Converter,” in *IEEE Transactions on Transportation Electrification*, 2018.

[11] C. Yu, J. Tamura and R. D. Lorenz, ”Optimum DC Bus Voltage Analysis and Calculation Method for Inverters/Motors With Variable DC Bus Voltage,” in IEEE Trans. on Industry Applications, 2013.

[12] A. Amerise, M. Mengoni, L. Zarri, A. Tani, S. Rubino and R. Bojoi, ”Open-ended induction motor drive with a floating capacitor bridge at variable DC link voltage,” *2017 IEEE Energy Conversion Congress and Exposition (ECCE)*, Cincinnati, OH, USA, 2017, pp. 3591-3597.

[13] L. Liu, G. Götting and J. Xie, ”Torque Ripple Reduction Using Variable DC-link Voltage Technique for Permanent Magnet Synchronous Motor in Battery Electric Vehicle,” *2020 IEEE 29th International Symposium on Industrial Electronics (ISIE)*, Delft, Netherlands, 2020, pp. 374-379.

[14] L. Liu, G. Goetting and J. Xie, ”Loss Minimization Using Variable DC-Link Voltage Technique for Permanent Magnet Synchronous Motor Traction System in Battery Electric Vehicle,” *2018 IEEE Vehicle Power and Propulsion Conference (VPPC)*, 2018, pp. 1-5.

[15] C. Pohlandt and M. Geimer, ”Variable DC-link voltage powertrain for electrified mobile work machines,” *2015 International Conference on Electrical Systems for Aircraft, Railway, Ship Propulsion and Road Vehicles (ESARS)*, Aachen, Germany, 2015, pp. 1-5.

[16] P. Pescetto and G. Pellegrino, ”Sensorless magnetic model and pm flux identification of synchronous drives at standstill,” *2017 IEEE International Symposium on Sensorless Control for Electrical Drives (SLED)*, Catania, Italy, 2017, pp. 79-84.

[17] https://www.brusa.biz/fileadmin/template/Produkte/Wandler/BRUSA_Factsheet_BDC546.pdf

[18] A. Sierra-Gonzalez, P. Pescetto, E. Trancho, E. Ibarra, G. Pellegrino, and F. Alvarez-Gonzalez ”Control of dual three-phase IPMSM drives with cascaded DC-link capacitors for third generation electric vehicles” *2021 IEEE Energy Conversion Congress and Exposition (ECCE)*, Vancouver, Canada, 2021.

[19] G. Pellegrino, R. I. Bojoi and P. Guglielmi, ”Unified Direct-Flux Vector Control for AC Motor Drives,” in *IEEE Transactions on Industry Applications*, vol. 47, no. 5, pp. 2093-2102, Sept.-Oct. 2011.

[20] E. Trancho, E. Ibarra, A. Arias, I. Kortabarria, J. Jurgens, L. Marengo, and A. Fricasse, “PM-assisted synchronous reluctance machine flux weakening control for EV and HEV applications,” *IEEE Transactions on Industrial Electronics*, vol. 65, no. 4, pp. 2986–2995, 2018.